Full wavefield migration, using internal multiples for undershooting

M. Davydenko and D.J. Verschuur, Delft University of Technology*

SUMMARY

Full wavefield migration (FWM) is an inversion-based imaging algorithm that utilizes the complete reflection measurements: primaries as well as all multiples, both surface and internal. Using multiples in the imaging can extend the illumination of the subsurface. In this paper we concentrate the study on the internal scattering that can be helpful in imaging structures from below that are otherwise difficult to image by primaries, i.e. an undershooting setting. This can be fruitful in the case of the obstacles, like oil-production facilities, or in the case of poor illumination, like sub-salt imaging or near-surface complexities. We demonstrate such approach on two synthetic examples.

INTRODUCTION

FWM can be referred to as a full waveform inversion process not in terms of velocities but in terms of reflectivities (Berkhout, 2012). Thus, the algorithm aims at minimizing the misfit between the modeled and the measured data by estimating the reflection coefficient at every gridpoint. The data is modeled by finite-summation algorithm in which the up- and downgoing wavefields are modeled separately one after another. Every sequence of downward and the following upward modeling will generate one additional order of scattering.

The modeling is based on one-way recursive propagation of the wavefields from one depth level to another, including possible scattering defined by the estimated reflection coefficients at each level. This means that in such modeling scheme the input velocity model is required only for the wavefield propagation and not for generating the internal scattering, as done in some RTM applications. Therefore, the input velocity model may not have sharp boundaries. This indicates the main difference in comparison to other migration algorithms which utilize multiples as well (Wong et al., 2012; Fleury and Snieder, 2011). In the next step, the separately modeled source-side up- and down-going wavefields are used in imaging with receiver-side down- and upgoing residual wavefields modeled in a similar way. Thus, in this scheme there are two pairs of wavefields responsible for the upside and downside imaging. Downside imaging can be used for undershooting purposes.

In Malcolm (2009) it was shown, that for the downside imaging it is required to downward back-propagate the measured wavefield, forward-propagate the source wavefield and store both wavefields at every level. Then the stored wavefields are multiplied by the local reflectivity, after which they are recursively propagated upward to every depth level and used for imaging, as shown in Figure 1a. In our approach both source-side and receiver-side wavefields can be modeled such that all transmission effects are included as well as all combination of multiple scattering can be generated (ee Figure 1b). Furthermore, the algorithm is applied in a full waveform inversion mode, where the estimated reflectivities are updated such that all input data is explained. The involved modeling scheme will be described in more detail in the next section.

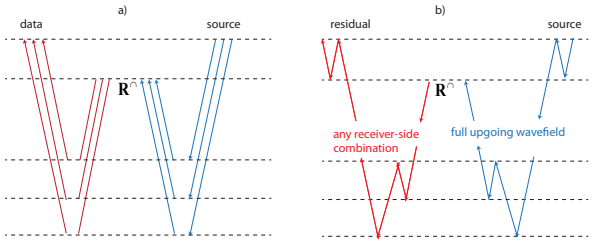

Figure 1: Schematic comparison of the method of the downside imaging proposed in Malcolm (2009) (a) and the method implemented in this paper (b). The blue path corresponds to the forward propagation from the source-side, the red path corresponds to the back-propagation from the receiver-side

THEORY

We follow the matrix notation (Berkhout, 1982) in which the monochromatic component of the seismic wavefield with the j-th source at depth level z_n and k-th receiver at depth level z_m can be represented as a scalar value $P_{jk}(z_m, z_n)$. Therefore, column-vector $\vec{P}_j(z_m, z_n)$ represents one shot record and matrix $\mathbf{P}(z_m, z_n)$ includes all shot records. By matrix $\mathbf{W}(z_m, z_n)$ we mean a monochromatic component for the propagation operator from depth level z_n to z_m. The reflectivity operator at depth level z_m is defined by matrix $\mathbf{R}(z_m, z_m)$.

FWM algorithm

In the FWM framework up- and downgoing wavefields at each depth level are considered. At depth level of consideration z_m incoming downgoing $\vec{P}_j^+(z_m, z_0)$ and upgoing $\vec{P}_j^-(z_m, z_0)$ wavefields approach this level from above and below, respectively. In the same manner two types of wavefields $\vec{Q}_j^+(z_m, z_0)$ and $\vec{Q}_j^-(z_m, z_0)$ leave the level to the up and down direction, respectively. Outgoing wavefields (Q) include the (possible) scattering obtained at the depth level z_m and become the incoming wavefield (P) at neighboring depth levels z_{m+1} and z_{m-1}. It can be written as follows (see also Figure 2):

$$\begin{aligned} \vec{P}^+(z_m, z_0) &= \mathbf{W}(z_m, z_{m-1})\vec{Q}^+(z_{m-1}, z_0) \\ \vec{P}^-(z_m, z_0) &= \mathbf{W}(z_m, z_{m+1})\vec{Q}^-(z_{m+1}, z_0). \end{aligned} \tag{1}$$

The total outgoing wavefield can be represented as a sum of the transmitted incoming wavefield in the same propagation direction and the reflected incoming wavefield from the opposite

DOI http://dx.doi.org/10.1190/segam2013-1413.1

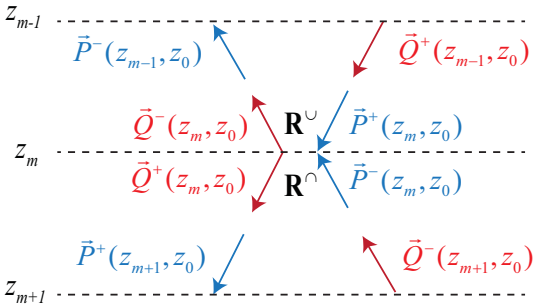

Figure 2: Wavefield relationship at arbitary depth lelel z_m

direction:

$$\begin{aligned}\vec{Q}^+(z_m,z_0) &= \vec{P}^+(z_m,z_0)+\delta\vec{P}(z_m,z_0)\\ \vec{Q}^-(z_m,z_0) &= \vec{P}^-(z_m,z_0)+\delta\vec{P}(z_m,z_0),\end{aligned} \tag{2}$$

where:

$$\delta\vec{P}(z_m,z_0)=\mathbf{R}^\cup(z_m,z_m)\vec{P}^+(z_m,z_0)+\mathbf{R}^\cap(z_m,z_m)\vec{P}^-(z_m,z_0) \tag{3}$$

is the two-way scattered wavefield. Moreover, the acoustic approximation simplifies Equation 3 such that:

$$\delta\vec{P}(z_m,z_0)=\mathbf{R}^\cup(z_m,z_m)[\vec{P}^+(z_m,z_0)-\vec{P}^-(z_m,z_0)]. \tag{4}$$

Thus, the upgoing and the downgoing wavefield can be recursively computed at any depth level z_m as follows:

$$\begin{aligned}\vec{P}^+(z_m,z_0) &= \mathbf{W}(z_m,z_0)\vec{S}^+(z_0,z_0)+\sum_{n=0}^{m-1}\mathbf{W}(z_m,z_n)\delta\vec{P}(z_n,z_0)\\ \vec{P}^-(z_m,z_0) &= \sum_{n=m+1}^{M}\mathbf{W}(z_m,z_n)\delta\vec{P}(z_n,z_0).\end{aligned} \tag{5}$$

Because $\delta\vec{P}$ term is dependent on P^+ and P^-, every new recalculation (roundtrip) will add a new order of scattering in the modeled upgoing and downgoing wavefields. Thus, we can control which order of scattering we would like to handle, which is an advantage compared to a finite-difference modeling scheme. As it was discussed before, FWM aims to estimate the reflectivity at each depth level by minimizing the cost function J which is the misfit $\Delta\mathbf{P}$ between the observed data P^-_{obs} and the data P^-_{mod} modeled by Equations 5:

$$J(\mathbf{R}^\cup,\mathbf{R}^\cap)=\sum_\omega||\mathbf{P}^-_{obs}(z_0,z_0)-\mathbf{P}^-_{mod}(z_0,z_0)||_2^2, \tag{6}$$

where:

$$\mathbf{P}^-_{mod}(z_0,z_0)=\sum_{n=0}^{N}\mathbf{W}(z_0,z_n)\delta\mathbf{P}(z_n,z_0) \tag{7}$$

We use a conjugate-gradient scheme to perform the minimization. For the upside reflection the gradient of J with respect to $\mathbf{R}^\cup$ will be:

$$\nabla J_{\mathbf{R}^\cup(z_m,z_m)}=\sum_\omega diag([\Delta\mathbf{P}^-(z_m,z_0)][\mathbf{P}^+(z_m,z_0)]^H), \tag{8}$$

where:

$$\Delta\mathbf{P}^-(z_m,z_0)=\mathbf{W}^H(z_m,z_0)\Delta\mathbf{P}^-(z_0,z_0) \tag{9}$$

can represents the back-propagated data residual to depth level z_m, where the image condition is applied.

Extension of the algorithm

However, in some situations one would like to estimate the downside reflection $\mathbf{R}^\cap$ separately. Therefore, the acoustic approximation has to be neglected. In this case the cost function becomes dependent on the both reflectivities $J(\mathbf{R}^\cup,\mathbf{R}^\cap)$ and an additional gradient should be included.

We propose to modify Equations 5 such that instead of the source wavefield we use the time-reversed residual data $\Delta\mathbf{P}^-(z_0,z_0)$ and perform the same modeling scheme:

$$\begin{aligned}\Delta P^-(z_m) &= \mathbf{W}^H(z_m,z_0)\Delta P^-(z_0)+\sum_{n=0}^{m-1}\mathbf{W}^H(z_m,z_n)\delta\vec{P}(z_n)\\ \Delta P^+(z_m) &= \sum_{n=m+1}^{M}\mathbf{W}^H(z_m,z_n)\delta\vec{P}(z_n),\end{aligned} \tag{10}$$

where:

$$\delta\vec{P}(z_n)=\mathbf{R}^\cup(z_n,z_n)\Delta\vec{P}^-(z_n)+\mathbf{R}^\cap(z_n)\Delta\vec{P}^+(z_n). \tag{11}$$

The receiver-side residual wavefields $\Delta\vec{P}^-(z_m,z_0)$ and $\Delta\vec{P}^+(z_m,z_0)$ can be considered as outcoming wavefields $\vec{Q}^-(z_m,z_0)$ and $\vec{Q}^+(z_m,z_0)$, respectively, as it was shown in Figure 2. The corresponding update of the downward reflectivity is given by:

$$\nabla J_{\mathbf{R}^\cap(z_m,z_m)}=\sum_\omega diag([\Delta\mathbf{P}^+_{obs}(z_n,z_0)][\mathbf{P}^-_{mod}(z_m,z_0)]^H). \tag{12}$$

Please note, that in a similar manner duplex imaging can also be implemented in the FWM algorithm (Davydenko and Verschuur, 2013). For this purpose the modeled upgoing wavefield can be cross-correlated with the back-propagated residual, from which additional image components related to structures close to the vertical can be computed (Malcolm et al., 2011; Marmalyevskyy et al., 2005; Xu and Jin, 2007; Jin et al., 2006).

EXAMPLES

In the following examples the data was modeled by an acoustic finite-difference modeling algorithm with non-free surface condition. Thus, the total observed wavefields consist of primaries and internal multiples.

Salt model example

DOI http://dx.doi.org/10.1190/segam2013-1413.1

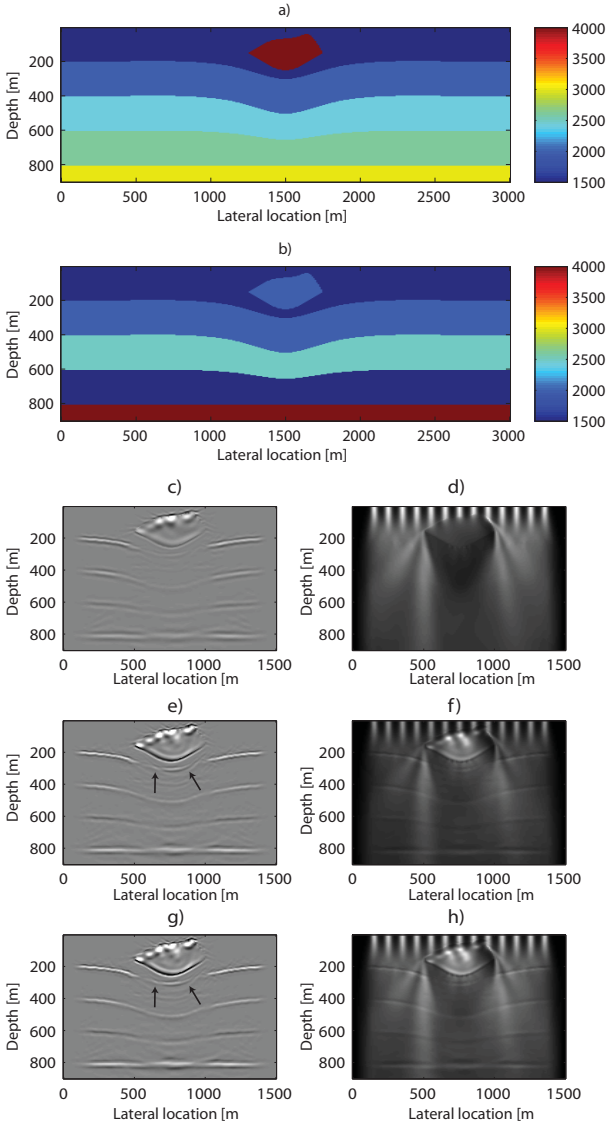

Figure 3: Results for the salt body example, for which the density and velocity model is given in a) and b). c) Pre-stack depth migration neglecting transmission effects; d) corresponding energy of the source wavefield; e) FWM image from primaries-only, f) corresponding illumination map; g) FWM image including internal multiples; f) corresponding illumination map).

Figure 3(a,b) shows the density and velocity models that were used as an input for the finite-difference modeling algorithm to generate the observed data.

In this model the salt-body forms an illumination obstruction zone, which is visible in Figure 3d. Figure 3c shows the image obtained by conventional pre-stack depth migration neglecting the transmission effects. The image resulting from the FWM algorithm using (modeling) primaries without including any internal multiples already shows an improvement in the sub-salt area (Figure 3e). The corresponding illumination map is shown in Figure 3f. The best result is obtained by including also the internal multiples in the FWM algorithm, confirmed by the reduced artifacts in Figure 3g and an improved illumination map in Figure 3h.

Near-surface example

In the second example we focus on the undershooting aspect of the extended FWM method, which can be used in case of obstacles at the surface or in the near surface. In the horizontally layered medium shown in Figure 4(a,b) we include near-surface anomaly, being a lens with different density and velocity. In case of using an incorrect migration velocity the image will be distorted below such anomaly. However, we demonstrate that if internal multiples would be used in the imaging such distortion can be overcome, because some internal multiples can propagate without passing through the anomaly and image the structure from below. For the sake of this demonstration we exclude all sources and receivers above the anomaly (from 1250m to 1750m) and perform the imaging in the following steps:

1. Using the usual FWM procedure with an acoustic approximation ($\mathbf{R}^{\cap} = -\mathbf{R}^{\cup}$) the estimate of $\mathbf{R}^{\cup}$ is computed.
2. Next, using the estimated reflectivity the primary-only dataset is computed and subtracted from the measured data. Thus, the residual wavefield with internal multiples is obtained.
3. Finally, the residual data containing internal multiples is imaged to obtain the downside reflection, i.e. updating of $\mathbf{R}^{\cap}$ ($\mathbf{R}^{\cup}$ is now fixed).

Figure 5a shows the estimated upside reflection while Figure 5b shows the estimated downside reflectivity in the top part of the model. Note that all boundaries in this area were imaged only via to the internal multiples. Using the imaged downside reflection coefficients, we can now generate an additional downgoing wavefield to illuminate the upside reflectivities again. Figure 5c showsthe first iteration result of the upside image ($\mathbf{R}^{\cup}$) revealed by internal multiples in the shallow region. Figures 5f-g display illumination maps of the various modeled wavefields. Figure 5d shows the illumination of the source wavefield in case of simple forward propagation. In the Figure 5e the illumination of the full downgoing wavefield is shown, the internal scattering has been added by the estimated $\mathbf{R}^{\cup}$ which was not estimated in the anomaly area. However, the illumination shown in Figure 5f from the modeled upgoing wavefield shows a much better illumination below the anomaly. Finally, the additional downward illumination formed by reflection (modeled by $\mathbf{R}^{\cap}$) of the upgoing modeled wavefield will also provide some energy below this

DOI http://dx.doi.org/10.1190/segam2013-1413.1

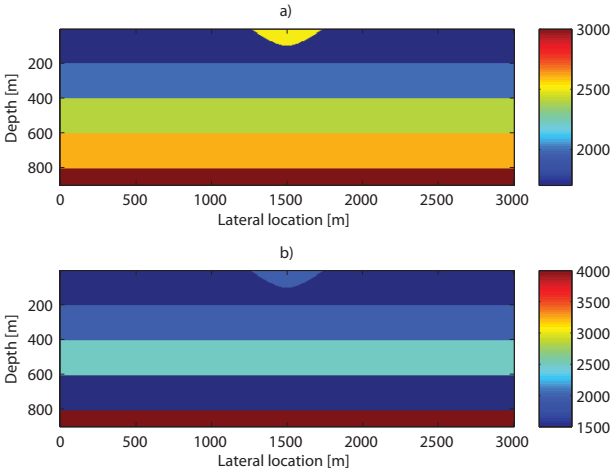

Figure 4: Density and velocity model for the second example representing near-surface anomaly

area (Figure 5g).

DISCUSSION

The current undershooting example has been shown in the situation when strong reflections in the subsurface generated the upgoing wavefield. In addition, including turning waves in the modeling scheme can enhance the downside imaging in case of positive velocity gradients when reflectors are not strong enough.

The downside imaging (undershooting) can also be helpful in the future development of elastic FWM version, in which ($\mathbf{R}^{\cup} \neq -\mathbf{R}^{\cap}$) and therefore $\mathbf{R}^{\cap}$ should be estimated separately as well.

CONCLUSIONS

The approach of underside imaging using and extension of the FWM algorithm was shown. In FWM all events in the seismic data - primaries and multiples - are used to illuminate the subsurface, where the last bounce of each reflection event is imaged. By back-propagation of the measured data via the imaged reflection energy in the subsurface in an upward fashion, it is also possible to estimate the reflectivity of certain structures from below. In this way it is possible to use multiply scattered events to retrieve information of the subsurface that is difficult to reveal by the primary illumination. The synthetic example with a complex near surface structure shows the potential of this method.

ACKNOWLEDGMENTS

The authors would like to thank sponsors of the Delphi consortium for their support.

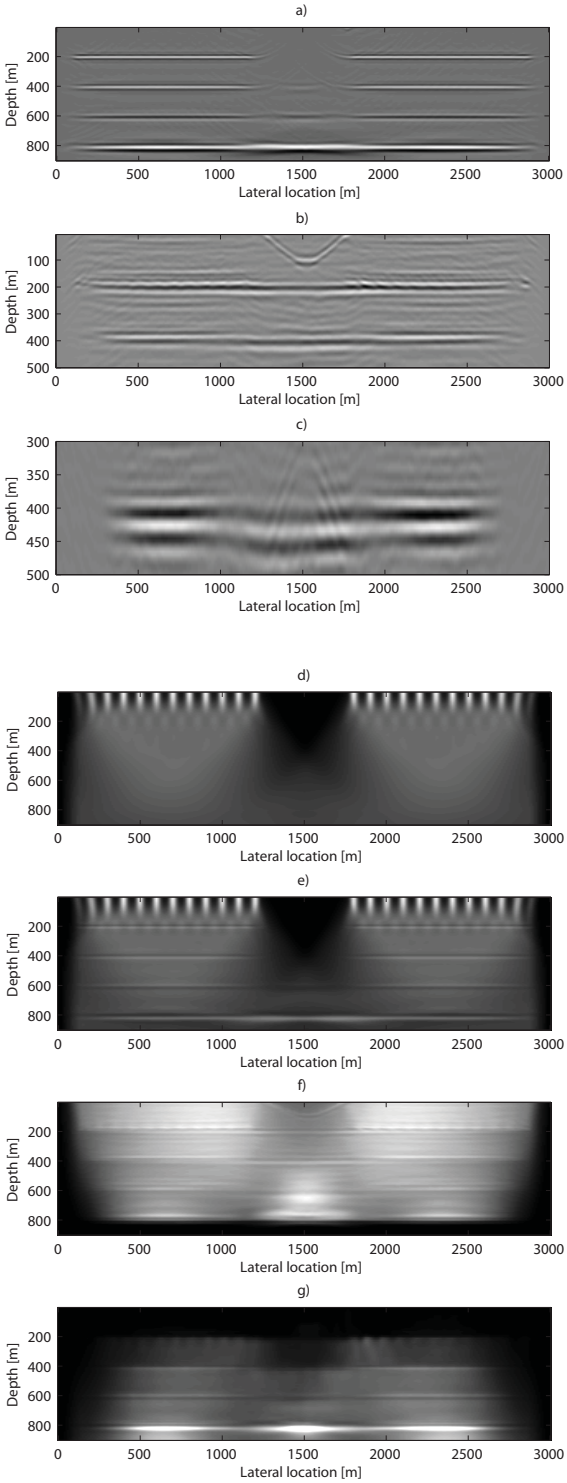

Figure 5: a) FWM upside image b) FWM downside image (imaging of internal multiples), c) Part of the downside image, revealed by internal multiples. Illumination maps of the d) extrapolated source e) estimated full downgoing wavefield, f) estimated downgoing wavefield, g) additional downgoing illumination (reflected upgoing wavefield)

DOI http://dx.doi.org/10.1190/segam2013-1413.1

http://dx.doi.org/10.1190/segam2013-1413.1

EDITED REFERENCES

Note: This reference list is a copy-edited version of the reference list submitted by the author. Reference lists for the 2013 SEG Technical Program Expanded Abstracts have been copy edited so that references provided with the online metadata for each paper will achieve a high degree of linking to cited sources that appear on the Web.

REFERENCES

Berkhout, A. J., 1982, Seismic migration, imaging of acoustic energy by wave field extrapolation, A: theoretical aspects: Elsevier (second edition).

Berkhout, A. J., 2012, Combining full wavefield migration and full waveform inversion, a glance into the future of seismic imaging: Geophysics, **77**, no. 2, S43–S50, http://dx.doi.org/10.1190/geo2011-0148.1.

Davydenko, M., and D. J. Verschuur, 2013, Full wavefield migration without dip limitation—Using duplex waves in the imaging with multiples: Presented at EAGE, Extended Abstracts.

Fleury, C., and R. Snieder, 2011, Reverse-time-migration of multiply scattered seismic waves: 81st Annual International Meeting, SEG, Expanded Abstracts, 3382–3387.

Jin, S., S. Xu, and D. Walraven, 2006, One-return wave equation migration: Imaging of duplex waves: 76th Annual International Meeting, SEG, Expanded Abstracts, 2338–2342.

Malcolm, A., B. Ursin, and M. V. de Hoop, 2008, Seismic imaging and illumination with internal multiples: Geophysical Journal International, http://dx.doi.org/10.1111/j.1365-246X.2008.03992.x.

Malcolm, A., M. V. de Hoop, and B. Ursin, 2011, Recursive imaging with multiply scattered waves using partial image regularization: A North Sea case study: Geophysics, **76**, no. 2, B33–B42.

Marmalyevskyy, N., Y. Roganov, Z. Gornyak, A. Kostyukevych, and V. Mershchiy, 2005, Migration of duplex waves: 75th Annual International Meeting, SEG, Expanded Abstracts, 2025–2028.

Wong, M., B. Biondi, and S. Ronen, 2012, Imaging with multiples using linearized full-wave inversion: 82nd Annual International Meeting, SEG, Expanded Abstracts, http://dx.doi.org/10.1190/segam2012-0864.1.

Xu, S., and S. Jin, 2007, An orthogonal one-return wave-equation migration: 77th Annual International Meeting, SEG, Expanded Abstracts, 2325–2329.